PROTEIN NANOCARRIER FOR TARGETED INTRACELLULAR

DELIVERY OF FUNCTIONAL ANTIBODIES

A Thesis
Presented to
The Academic Faculty

by

Cyril Igorevich Lukianov

In Partial Fulfillment
of the Requirements for the Degree
Bachelor of Science with the Research Option in the
School of Chemical and Biomolecular Engineering

Georgia Institute of Technology
May 2017

PROTEIN NANOCARRIER FOR TARGETED INTRACELLULAR

DELIVERY OF FUNCTIONAL ANTIBODIES

Approved by:

Dr. Julie Champion, Advisor
School of Chemical and Biomolecular Engineering
Georgia Institute of Technology

Dr. Ravi Kane
School of Chemical and Biomolecular Engineering
Georgia Institute of Technology

Dr. Corey Wilson
School of Chemical and Biomolecular Engineering
Georgia Institute of Technology

Date Approved: 05/01/2017

ACKNOWLEDGEMENTS

TABLE OF CONTENTS

LIST OF FIGURES

Page

NOMENCLATURE

ADC	Antibody-Drug Conjugate
SPAB	Staphylococcal Protein A, Domain B
iRGD	internalizing RGD
CendR	C end Rule
IgGRb	Rabbit Immunoglobulin G
IgGMs	Mouse Immunoglobulin G
HER2	Human Epidermal Growth Factor Receptor 2

SUMMARY

The cell membrane remains a formidable barrier for antibody-based therapies, and efficient intracellular delivery of functional antibodies may be critical for modulating intracellular signaling mechanisms and protein-protein interactions involved in various disorders. This study utilized protein engineering techniques to develop a novel nanocarrier that is capable of delivering functional antibodies to the intracellular environment. Each nanocarrier contains six SPAB antibody-binding domains, and is therefore capable of delivering up to six antibodies. The interaction between the SPAB domain of the nanocarrier and the heavy chain constant region of the antibody is noncovalent, thus allowing the nanocarrier to bind different functional antibodies with the same affinity. Three iRGD domains were integrated into the nanocarrier structure to allow for selective targeting of integrin-overexpressing cells. We successfully expressed the protein monomers, assembled the functional nanocarrier, and investigated its antibody-binding properties. Results of cellular uptake studies involving HeLa, MCF-7, as well as SK-BR-3 cancer cell lines indicate significant cellular uptake of antibody-loaded nanocarrier as compared to soluble antibody control. Without any modification of the carrier, we also used HER2 targeting antibodies to direct the carriers preferentially into HER2-positive SK-BR-3 cells. In addition to efficient cellular uptake, the highly biocompatible and modular nature of our nanocarrier makes it ideal for expanding the scope of antibody-based therapeutics to the intracellular environment.

CHAPTER 1

INTRODUCTION

Various cancers remain among the leading causes of death in the United States,
and although the mortality rates for most cancers have stabilized or decreased, liver and
pancreatic cancer mortality rates have increased for both men and women [1]. The
National Cancer Institute estimates that about 40 percent of adult men and women in the
United States will be diagnosed with some type of cancer in their lifetime [1]. Antibody-
drug conjugates (ADCs) are a novel treatment option for several disorders, including
some cancers [2]. The U.S. Food and Drug Administration (FDA) recently approved
several ADCs for treatment of lymphoma and leukemia [2].

Most ADCs, both FDA-approved and in development, utilize the antibody as a
targeting moiety, relying on antibody binding to specific cell-surface receptors that are
overexpressed by the specific cancer cells [2]. Antibody-receptor interactions then allow
the ADC to be internalized by the cancer cell, resulting in drug release from the ADC
inside the target cancer cell [2]. Current FDA-approved ADCs usually carry between 1
and 8 small molecule drugs, but some prospective ADCs are comprised of a targeting
antibody covalently linked to polymers or nanoparticles, thus allowing for targeted
delivery of larger cargo molecules [2,3]. Several current and future ADC designs utilize
stimulus-responsive covalent-linkers, such as those that may be cleaved by proteases
once the cell internalizes the ADC, in order to achieve more sustained cargo release as
well as lower toxicity towards healthy cells [4]. To further enhance the targeting

properties of ADCs, biparatopic rather than monoclonal antibodies have also been utilized [5].

ADCs have already shown significant potential as cancer therapeutics, however, one of the limitations of the current design is its reliance on a single antibody chemically conjugated to a single drug moiety or nanoparticle. Different cancer cells have many diverse mutations which result in overexpression of various cell-surface receptors, and although many overexpressed receptors, such as EGFR, are common to many cancer cell types, the current approach to ADC design may require the development of a separate ADC for each specific receptor, cancer cell type, as well as drug entity [3,6]. Another shortcoming of current ADC constructs is their use of antibodies as targeting moieties, rather than as possible therapeutic agents themselves. It was previously shown that antibodies may be used to modulate oncoprotein interactions inside cancer cells, and thus may be considered as viable chemotherapeutic agents [7,8].

We have previously described a protein nanocarrier that may be used for intracellular delivery of up to six functional antibodies [9]. The carrier exhibits low toxicity and high cytosolic delivery efficiency [9]. The goal of this thesis is to enhance the original nanocarrier design to achieve specific targeting ability. The end goal is delivery of functional, therapeutic antibodies to the intracellular environment of specific cell and tissue types. We considered two approaches to targeting: introduction of targeting peptide domains, as well as the use of targeting antibodies. A truly modular and specific nanocarrier design could expand the scope of antibody-based therapeutics to the intracellular environment.

CHAPTER 2

LITERATURE REVIEW

Antibody drug conjugates (ADCs) are a novel class of truly biocompatible and highly specific therapeutics, with several already approved by the U.S. Food and Drug Administration (FDA) for treatment of various disorders, including cancers such as lymphoma [2].Most currently used ADCs utilize the antibody as a targeting agent, and thus rely on the conjugate binding to the specific cell surface receptor to initiate cellular uptake and subsequent intracellular drug release for achieving their therapeutic goals [2].

Several ADCs that are currently in development also utilize the antibody as a targeting moiety, but are able to deliver much larger and complex cargo molecules, such as nanoparticles, rather than smaller drug molecules. As reported by Palanca-Wessels et al., polymeric micelle nanoparticles loaded with siRNA molecules may be conjugated with specific targeting antibodies to enhance particle delivery to target cancer cells [3]. The study utilized antibodies specific for HER2 receptors, which are receptor tyrosine kinases known to be overexpressed by many types of cancer cells [3]. Targeted delivery of siRNA may be more therapeutically efficient than small molecule drug delivery, since siRNA is used to knockdown specific oncogenes responsible for the cancerous properties of the cell, while maintaining relatively low toxicity to healthy cells in the surrounding tissues [3]. The shape and structure of the nanoparticle also enhance the cytosolic delivery of the cargo through better endosomal escape as compared to small molecule drugs. However, the experimental results show significant uptake of nanoparticles that have not been conjugated with the targeting antibody, and thus the targeting efficiency of

this new design may be inconsistent. This design also relies on electrostatic interactions between siRNA and the nanoparticle backbone, and thus may behave differently in different tumor microenvironments.

In order to achieve better targeting efficiency, several other novel ADC designs rely on biparatopic antibodies, which are engineered from the variable regions of two different monoclonal antibodies. Li et al. showed that an ADC composed of a biparatopic HER2-specific antibody conjugated to a microtubule-stabilizing agent achieved superior cytotoxic effects as compared to a current FDA-approved monoclonal analogue [5]. Their results indicate that the use of a biparatopic antibody promotes receptor clustering and thus enhances cellular uptake and subsequent endosomal degradation of the overexpressed receptors [5]. However, an immunoblotting analysis of cell lysate may not be sufficient for accurately determining whether the HER-2 receptors are truly degraded following internalization, and therefore the authors' final conclusions do not seem well supported.

Another novel method of enhancing targeting efficiency of ADCs involves the use of sensitive linker molecules, most of which either respond to chemical and physical changes in the microenvironment, or interact directly with chemical agents. Several pH-sensitive linkers and monomers have been described, many of which take advantage of the slight decrease in pH in tumor microenvironments that is the direct result of the Warburg effect: increased anaerobic glycolysis rate in cancer cells [10]. Although pH sensitivity may be a viable way of achieving tumor targeting, pH changes may be too subtle initially and may only be sufficient for targeting once the cancer has progressed substantially.

Several other studies have introduced a different approach: the use of enzyme-responsive linkers and monomers. These nanoparticles and ADCs achieve targeted drug release due to cleavage of the linker by enzymes that are present either in the surrounding extracellular environment or within intracellular vesicles. Lehar et al. have proposed an ADC containing an enzyme-sensitive linker for delivery of antibiotics to methicillin-resistant *S. aureus* (MRSA) bacteria that are located inside the phagolysosomes of macrophages [4]. Although most MRSA that are phagocytized by macrophages and neutrophils are rapidly cleared, some may be retained and transported throughout the body, thus contributing to recurring infections [4]. Therefore, MRSA trapped inside the phagolysosomes of macrophages may act as "Trojan horses" and effectively evade conventional antibiotic treatments [4]. The ADC design proposed by Lehar et al. effectively overcomes limitations of conventional antibiotics for treatment of intracellular MRSA [4]. Targeting is achieved through a specific antibody that binds MRSA, and the cytotoxic effect is achieved through proteasomal cleavage of the linker between the antibody and the antibiotic drug molecule inside the phagolysosome [4]. *In vitro* experiments on murine macrophages as well as *in vivo* tests on mice with bacteraemia indicate an advantage of this ADC design as compared to conventional antibiotic treatment [4]. This novel idea may have many potential applications and allows for more efficient and targeted delivery, while also minimizing potential side effects since the cargo molecule remains inactive until the sensitive linker is cleaved in the vicinity of its target.

Although numerous ADC designs have already been tested and many are currently in development, most of these conjugates fail to take advantage of the

therapeutic potential of antibodies themselves. High specificity, extended half-life in circulation, as well as excellent biocompatibility makes antibodies very suitable therapeutic agents [7]. Antibodies have been shown to play significant roles in cellular signaling pathways and protein-protein interactions, including mechanisms involved in progression of various diseases [7,8]. A major obstacle to antibody-based therapy, however, is the efficient cytosolic delivery of functional antibodies.

Many current methods of intracellular delivery of functional antibodies require initial permeabilization of the cell membrane, thus rendering the cell nonviable [11]. Other methods of delivering functional antibodies to live cells involve the use of silica-based nanoparticles, but the loading of IgG onto the nanoparticle is very low (1.26 μg IgG/mg) [12]. The relatively low loading efficiency may be overcome by the use of virus-like particles, but immunogenicity remains a major concern for potential therapeutic uses. [13] Thus, a novel approach is necessary in order to expand the scope of antibody-based therapies to cytosolic targets.

We have previously described a protein nanocarrier that may be used for intracellular delivery of up to six functional antibodies [9]. The nanocarrier contains two functional domains: a hexameric CC-HEX peptide that is formed through self- assembly of six α-helical domains into a coiled coil and the Staphylococcal protein A domain B (SPAB) that may non-covalently bind different antibodies with different affinities [16,17]. The CC-HEX peptide has good long-term stability and self-assembly properties, making it ideal for easy assembly of various domains into a complete, functional nanocarrier. The SPAB domain has good affinity for many human antibodies and binds them non-covalently, thus eliminating the need for complex chemical conjugation. The

6

functional nanoparticle has a central CC-HEX peptide linked to six SPAB domains, and is theoretically capable of delivering six functional antibodies to the intracellular environment. The goal of the current study is to increase the targeting specificity of the original HEX nanocarrier in order to enable intracellular antibody delivery to specific cancer cell types.

Effective and efficient cytosolic delivery of large biological macromolecules, such as antibodies, may be facilitated by addition of various peptide domains to the conjugate or nanoparticle structure. One such domain, internalizing RGD (iRGD) has been shown to enhance the delivery and tumor penetration of a nanoparticle containing the variable domain from the heavy chain of an anti-EGFR antibody, which binds human epidermal growth factor receptors [14]. The iRGD domain contains the amino acids arginine (R), glycine (G), and aspartic acid (D), which are well known for their affinity for $\alpha v\beta 3$ and $\alpha v\beta 5$ integrins, as well as a CendR motif, which interacts with the receptor Neuropilin-1 (NRP-1), triggering the internalization cascade [14]. The $\alpha v\beta 3$ and $\alpha v\beta 5$ integrins are overexpressed in many cancers, and such may be potential therapeutic targets [14,15]. Sha et al. demonstrated that addition of the iRGD domain substantially increased the penetration of the nanoparticle into deeper layers of tumor tissue, as indicated by confocal microscopy images of 3D multicellular spheroids that were incubated with the nanoparticle [14]. Although the authors state that the exact molecular mechanism for iRGD's targeting and tumor penetration is yet unknown, the experimental results also indicate substantial antitumor activity of the anti-EGFR-iRGD peptide without addition of any drug molecules [14].

Niikura, Horisawa, and Doi have also introduced additional peptide domains to

the anti-EGFR antibody; however, the B18 and B55 fusogenic peptides do not affect targeting properties, but rather increase the efficiency of endosomal escape [6]. Release of large molecules from endosomal vesicles is a critical step for cytosolic targeting, and remains a major obstacle for intracellular delivery of functional antibodies. B18 and B55 have previously been shown to increase endosomal escape of smaller peptides through conformational changes at acidic pH, and Niikura et al. showed very similar results for the anti-EGFR antibody fragment.

In this thesis, we investigated both the use of targeting peptide domains as well as HER2 receptor targeting antibodies. Introduction of the iRGD domain should allow the particle to bind and deliver non-targeting antibodies while still maintaining specific targeting as well as tissue-layer penetration properties. Anti-HER2 monoclonal antibodies have been approved by the FDA as viable agents for targeted breast cancer therapy and may be used in conjunction with our nanocarrier to achieve not only better targeting, but also increased anti-tumor efficacy [22]. The use of these targeting antibodies does not necessitate any changes in the design of the nanocarrier, but may require additional investigation of loading efficiency.

CHAPTER 3

MATERIALS AND METHODS

3.1   Plasmid Preparation and Site-Directed Mutagenesis:

Bacterial expression vectors pQE80-SPAB-HEX and pQE80-HEX-SPAB were synthesized by GenScript (Piscataway, NJ). The plasmid encoding SPAB-HEX-iRGD was prepared by site-directed mutagenesis of pQE80-SPAB-HEX. DNA primers were purchased from Eurofins Genomics (Louisville, KY). Phusion® High Fidelity DNA Polymerase, reaction buffers, and the deoxynucleotide (dNTP) solution mix were purchased from New England BioLabs (Ipswich, MA). TOP10 *Escherichia Coli (E. Coli)* were transformed with pQE80-SPAB-HEX-iRGD, pQE80-SPAB-HEX and pQE80-HEX-SPAB.

3.2   Protein Expression and Purification:

HEX-SPAB, SPAB-HEX, and SPAB-HEX-iRGD were expressed in TOP10 *E. Coli* that have acquired the appropriate plasmid vector through bacterial transformation. *E. Coli* cells were cultured in Lysogeny Broth (LB) media. Protein expression was induced by addition of isopropyl β-D-1-thiogalactopyranoside (IPTG) once the optical density (OD) of the cell culture measured by the NanoDrop® spectrophotometer at 600 nm has reached 0.6 [18]. The cells were then harvested by centrifugation, suspended in lysis buffer and further disrupted by sonication. The resulting cell lysate was separated using centrifugation; the supernatant was collected and purified using nickel–nitrilotriacetic acid (Ni-NTA) affinity chromatography under native conditions.

A total of ten eluted fractions were collected for each recombinant protein, and the concentration of each fraction was determined by the NanoDrop® spectrophotometer using the absorbance at 280 nm and known values of molecular weight and extinction coefficient (ε) of CC-HEX [16,18]. Fractions that contained less than 0.5 mg/mL of target protein were discarded. The first eluted fraction for each protein was also discarded due to high likelihood of presence of unwanted contaminant proteins. A PD-10 desalting column was used to exchange the buffer of the protein solutions from elution buffer to 1x phosphate buffered saline (PBS) [19].

The purity of the eluted fractions was analyzed by sodium dodecyl sulfate-polyacrylamide gel electrophoresis (SDS-PAGE). The size of HEX-SPAB, SPAB-HEX, and SPAB-HEX-iRGD was characterized using dynamic light scattering (DLS), and verified using the known size values for CC-HEX and SPAB [16,17,20].

3.3   Assembly of Functional Nanocarriers (HEX and HEX-iRGD):

To produce the functional HEX nanocarrier, HEX-SPAB and SPAB-HEX recombinant proteins were initially mixed together at a molar ratio of 1:1 and denatured by addition of 10% by volume sodium dodecyl sulfate (SDS). The same procedure was followed to assemble the HEX-iRGD nanocarrier, with the only exception being the use of SPAB-HEX-iRGD instead of SPAB-HEX. The mixtures were allowed a total reaction time of 30 minutes to ensure complete disassembly of HEX-SPAB, SPAB-HEX, and SPAB-HEX-iRGD into their constituent monomeric peptides. The functional nanocarriers were then fabricated by reassembly of recombinant proteins into their hexameric state due to removal of SDS. PD-10 desalting columns as well as the ÄKTA fast protein liquid

chromatography (FPLC) system were used to completely remove SDS [19,21]. Purity of the resulting reassembled nanocarriers (HEX and HEX-iRGD) was verified using SDS-PAGE. Proper assembly was also verified through size measurement using DLS [20].

3.4   Antibody Binding:

Size of HEX, HEX-iRGD, and rabbit immunoglobulin G (IgGRb) was measured using DLS [20]. Concentration of HEX and HEX-iRGD monomers as well as IgGRb was determined by the NanoDrop® spectrophotometer using the absorbance at 280 nm and known values of molecular weight and extinction coefficient (ε) of CC-HEX and IgGRb [16,18]. Several samples containing various molar ratios of HEX:IgGRb were prepared by mixing appropriate volumes of HEX and IgGRb and vortexing to ensure even mixing. Size of the HEX-IgGRb nanocarriers was measured using DLS [20].

3.5   Cellular Uptake Studies: HEX/HEX-iRGD + IgGRb

HeLa, MCF-7, and SK-BR-3 cells were cultured in complete media supplemented with 10% fetal bovine serum (FBS) at 37°C and 5% CO_2 for 24 hours. The cells were then dissociated from the culture flask by addition of 0.25% trypsin, and cell density was determined by counting cells using a hemocytometer. The cells were then transferred to a 96-well plate at a seeding density of 10,000 cells per well.

IgGRb labeled with TAMRA red fluorescent dye was obtained from stock, and bound to HEX or HEX-iRGD as previously described. The appropriate volume of HEX-IgGRb-Dye solution was mixed with complete media to bring the total volume of each well to 100 µL. The working concentrations were 0.7 µM and 1.4 µM for HEX, IgGRb-TAMRA,

respectively. The cells were incubated at 37°C and 5% CO_2 for 24 hours, and visualized using fluorescence microscopy. All fluorescence microscopy images were collected at the same exposure time using a 10X magnification optical lens.

3.6   Integrin Targeting Study

Anti-integrin $\alpha v \beta 3$ antibodies were purchased from EMD Millipore (Billerica, MA). To investigate the efficiency of integrin targeting by HEX-iRGD, fixed HeLa cells were pre-incubated with soluble anti-integrin $\alpha v \beta 3$ antibodies for 1 hour according to the manufacturer's protocol. The cells were then washed and incubated with a solution of HEX + IgGRb or HEX-iRGD + IgGRb with or without anti-integrin $\alpha v \beta 3$ antibodies for 24 hours. The working concentrations were 0.7 μM for HEX/HEX-iRGD and 1.4 μM for IgGRb-TAMRA. A secondary anti-rabbit fluorescent antibody was used to visualize integrin binding of the primary antibody, and thus confirm its effectiveness as an $\alpha v \beta 3$ blocking agent. Cells were visualized using fluorescence microscopy. All fluorescence microscopy images were collected at the same exposure time using a 10X magnification optical lens.

3.7   HER2 Targeting Study

Anti-HER2 antibodies were purchased from Sigma Aldrich (St. Louis, MO). MCF-7, and SK-BR-3 cells were cultured in complete media supplemented with 10% fetal bovine serum (FBS) at 37°C and 5% CO_2 for 24 hours. The cells were then dissociated from the culture flask by addition of 0.25% trypsin, and cell density was determined by counting cells using a hemocytometer. The cells were then transferred to a 96-well plate at a

seeding density of 10,000 cells per well.

Samples were prepared by mixing an appropriate volume of HEX, IgGRb-TAMRA, and/or anti-HER2 in serum-free media, with subsequent addition of FBS after 5-10 minutes to allow sufficient time for HEX-antibody binding. The working concentrations were 0.2 μM, 0.4 μM, and 0.4 μM for HEX, IgGRb-TAMRA, and anti-HER2, respectively. Samples containing no anti-HER2 antibodies were supplemented with unlabeled rabbit IgG, in order to maintain an equal concentration of fluorescent antibody across all samples. Cells were incubated with the sample solutions for 10 hours and washed 3 times with sterile 1X PBS. The mean fluorescence intensity per well was then measured using a microplate reader and the cells were imaged using a fluorescent microscope. All fluorescence microscopy images were collected at the same exposure time using a 10X magnification optical lens.

CHAPTER 4

EXPERIMENTAL RESULTS

4.1   Purification of Recombinant Proteins and Assembly of Functional Nanocarriers

The recombinant peptides SPAB-HEX, SPAB-HEX-iRGD, as well as HEX-SPAB were

successfully expressed in *E. Coli*, and purified from cell lysate under native conditions.

SDS-PAGE analysis of several eluted fractions shown in Figure 1 indicates high purity,

and the apparent molecular weight readings coincide with the known values. It is worth

noting the lower expression yield of HEX-SPAB, which was almost five times less than

that of SPAB-HEX and SPAB-HEX-iRGD. Results shown in Figure 2 indicate successful

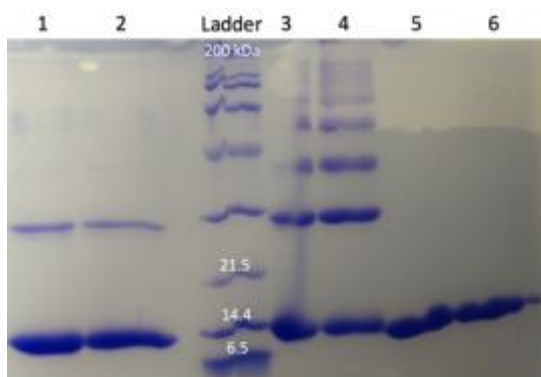assembly of the functional HEX-iRGD nanocarrier.

Figure 1. SDS PAGE analysis of SPAB-HEX-iRGD (1,2,3,&4) and HEX-SPAB(5&6) elutions.
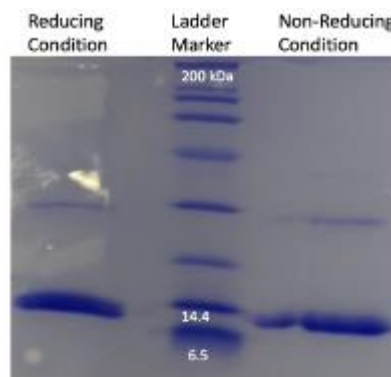
Figure 2. SDS PAGE analysis of assembled HEX-iRGD nanocarrier.

4.2   Binding of IgGRb to HEX-iRGD:

Size of purified 10 µM HEX-iRGD and IgGRb was determined using DLS. Intensity-

based size distribution measurements presented in Figure 3 indicate an average size of 18

nm for HEX-iRGD and 15 nm for IgGRb. The study of the concentration dependence of

14

nanocarrier size indicates greater average particle size at higher ratios of HEX:IgGRb, as

presented in Figure 3. Nanocarrier size was measured using DLS. A noteworthy

observation, as shown in Figure A2, is the broad nature of the peaks at higher ratios of

HEX:IgGRb, possibly indicating a more diverse population of IgGRb-bound nanocarrier
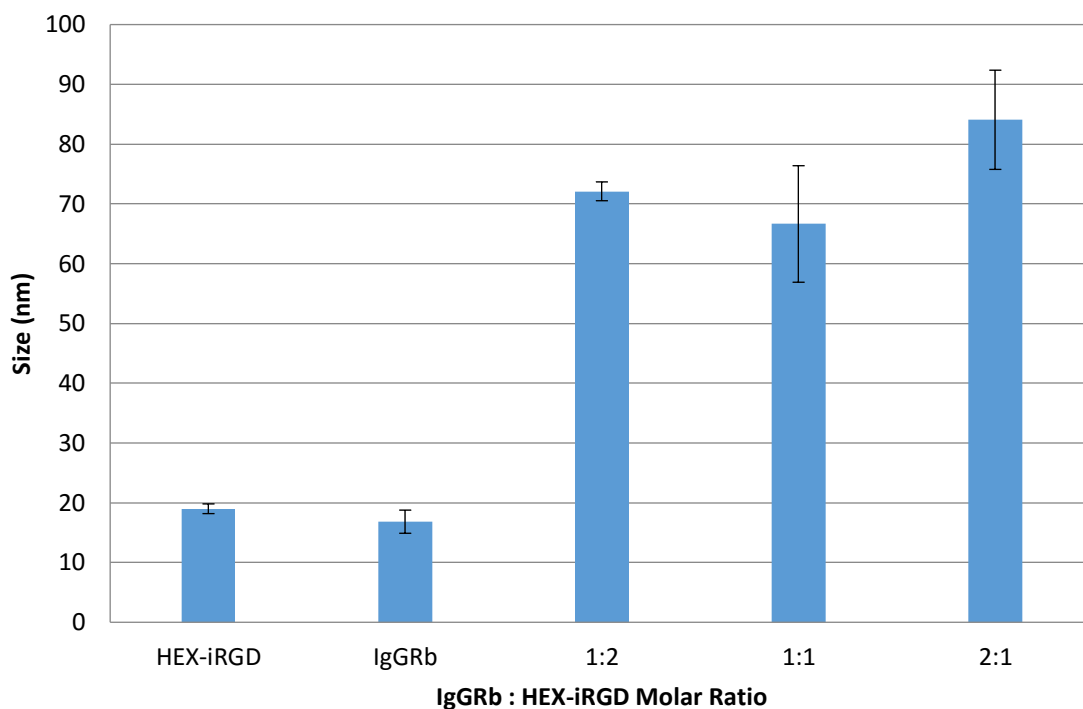
species.

Figure 3. DLS size measurements of HEX-iRGD + IgGRb at different molar ratios.

4.3   *Cellular Uptake Study: HEX + IgGRb*

HeLa cells were cultured in complete media supplemented with 10% fetal bovine serum

(FBS) at 37°C and 5% CO_2 for 24 hours. IgGRb labeled with TAMRA red fluorescent

dye was obtained from stock, and bound to HEX or HEX-iRGD as previously described.

The working concentrations were 0.7 μM and 0.9 μM for IgGRb-TAMRA, and 1.4 μM

and 1.9 μM for HEX. The cells were incubated at 37°C and 5% CO_2 for 24 hours, and

visualized using fluorescence microscopy. All fluorescence microscopy images were collected at the same exposure time.

Fluorescence microscopy images presented in Figure 4 indicate increased uptake of HEX-IgGRb-TAMRA nanocarrier as compared to soluble IgGRb-TAMRA. The images also indicate a dose-dependence of uptake, with the higher-concentration sample showing a stronger fluorescent signal. The negative control group was treated with neither HEX nor IgGRb and therefore shows no fluorescent signals. Incubation with nanocarrier did not seem to have any negative effects on the morphology of HeLa cells.
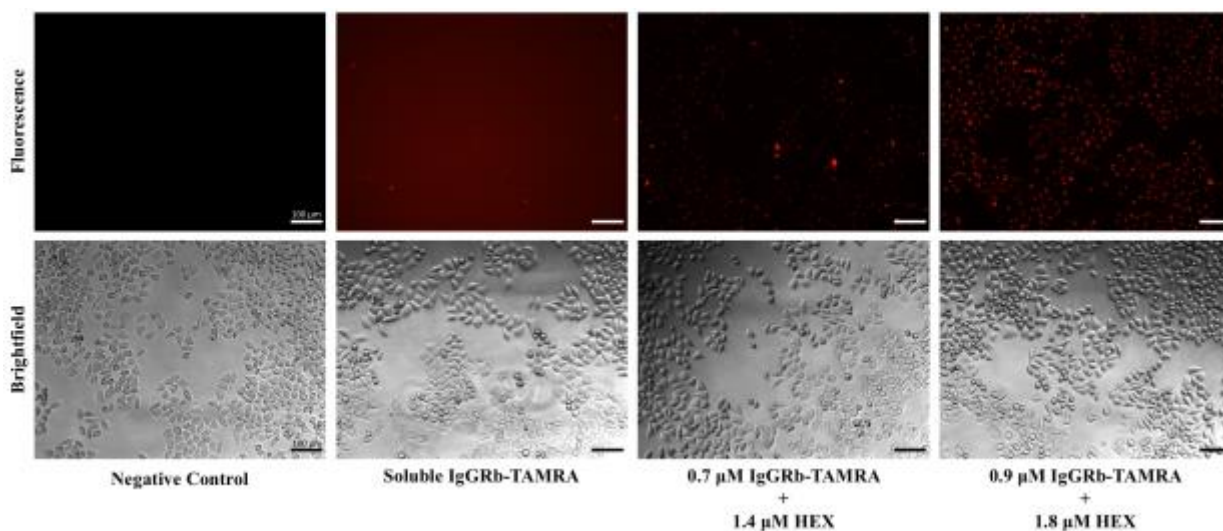

Figure 4. Fluorescence microscopy images of concentration-dependent cellular uptake of HEX-TAMRA and HEX-IgGRb-TAMRA by HeLa cells. The scale bar represents 100 μm.

4.4   Cellular Uptake Study: HEX + IgGRb vs. HEX-iRGD + IgGRb

HeLa, MCF-7, and SK-BR-3 cells were cultured in complete media supplemented with 10% fetal bovine serum (FBS) at 37°C and 5% CO_2 for 24 hours. IgGRb labeled with TAMRA red fluorescent dye was obtained from stock, and bound to HEX or HEX-iRGD as previously described. The working concentrations were 0.7 μM for IgGRb-TAMRA, and 1.4 μM for HEX. The cells were incubated at 37°C and 5% CO_2 for 24 hours, and

16

visualized using fluorescence microscopy. All fluorescence microscopy images were collected at the same exposure time.

Microscopy images shown in Figure 5 indicate a difference in uptake of HEX-IgGRb and HEX-iRGD-IgGRb by Hela, MCF-7, and SK-BR-3 cells. The intensity of the fluorescent signal is evidently stronger for HEX-iRGD-IgGRb as compared to HEX-IgGRb. However, flow cytometry data shown in Figure A1 indicate that this difference is not significant, and therefore may not be attributed to enhanced targeting or internalization of HEX-iRGD. It is also worth noting the difference in uptake pattern between the three cell lines. Fluorescent signals in MCF-7 cells tends to be concentrated in a smaller number of cells, while HeLa and SK-BR-3 cells show a more uniform distribution across cells.

To confirm that the observed fluorescent signal does indeed correspond to uptake and not membrane interactions, the efficiency of the cell washing protocol was investigated. SK-BR-3 and MCF-7 cells were incubated with solutions of HEX+IgGRb-TAMRA at 4 °C for 24 hours. The cells were then subject to washing protocols of varying rigor, collected by adding trypsin and analyzed on the flow cytometer. The results shown in Figure A5. indicate no significant difference between cells that were not incubated with HEX-IgGRb-TAMRA (Negative Control), and cells subjected either to the regular washing protocol (3 washes with 1X PBS), or the extra washing protocol (7 washes with 1X PBS). There is, however, a pronounced difference between the previously mentioned samples and cells that were not washed at all. This result confirms that the standard washing protocol is effective for removing any nanocarriers that adhere to the cell membrane. Thus, it may be concluded that fluorescence microscopy data are indicative of cellular uptake of the nanocarriers.
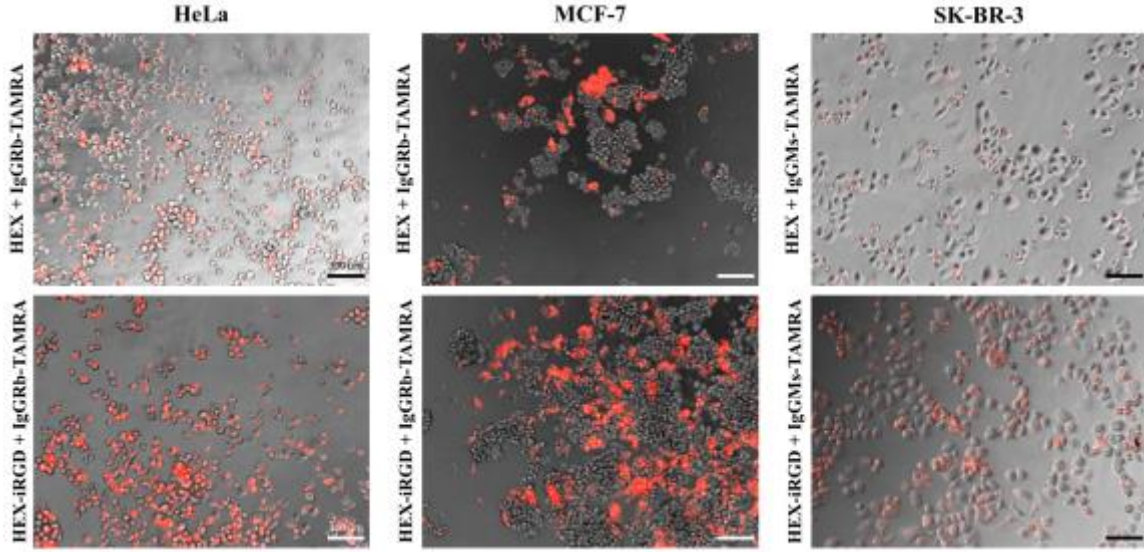
Figure 5. Fluorescence microscopy images showing uptake patterns of HEX + IgG-TAMRA and HEX-iRGD + IgG-TAMRA by HeLa, MCF-7 cells, and SK-BR-3 cells. The scale bar represents 100 μm.

4.5   *Integrin Targeting Study: HEX + IgGRb vs. HEX-iRGD + IgGRb*

To investigate the efficiency of integrin targeting by HEX-iRGD, fixed HeLa cells were pre-incubated with soluble anti-integrin $\alpha v \beta 3$ antibodies for 1 hour according to the manufacturer's protocol. The cells were then washed and incubated with a solution of HEX + IgGRb or HEX-iRGD + IgGRb with or without anti-integrin $\alpha v \beta 3$ antibodies for 24 hours. The working concentrations were 0.7 μM for HEX/HEX-iRGD and 1.4 μM for IgGRb-TAMRA. A secondary anti-rabbit fluorescent antibody was used to visualize integrin binding of the primary antibody, as shown in Figure A6, and thus confirm its effectiveness as an $\alpha v \beta 3$ blocking agent. Cells were visualized using fluorescence microscopy. All fluorescence microscopy images were collected at the same exposure time.

18

Microscopy images presented in Figure 6 show no significant difference in membrane interactions of HEX and HEX-iRGD either in the presence or absence of anti-integrin αvβ3 antibodies.
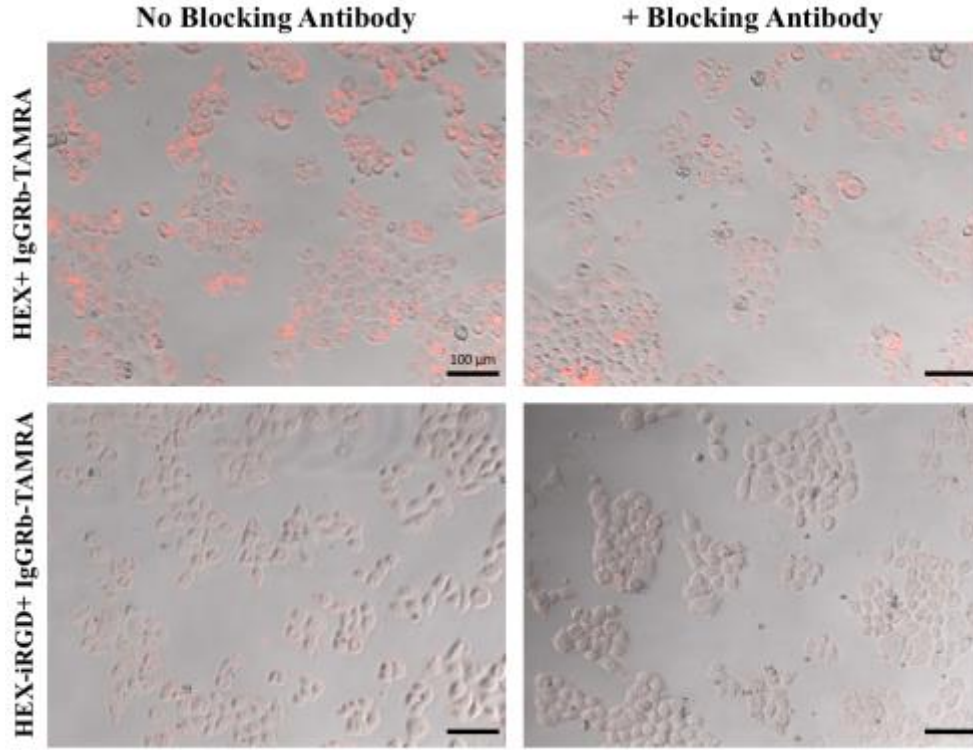

Figure 6. Fluorescence microscopy images showing membrane interaction patterns of HEX-IgGRb and HEX-iRGD-IgGRb by fixed HeLa cells in the presence or absence of anti-integrin αvβ3 antibodies. The scale bar represents 100 μm.

4.6   HER2 Receptor Targeting

MCF-7 and SK-BR-3 cells were cultured in complete media supplemented with 10% fetal bovine serum (FBS) at 37°C and 5% CO_2 for 24 hours. The working concentrations were 0.2 μM, 0.4 μM, and 0.4 μM for HEX, IgGRb-TAMRA, and anti-HER2, respectively. Samples containing no anti-HER2 antibodies were supplemented with unlabeled rabbit IgG, in order to maintain an equal concentration of fluorescent antibody across all samples. Cells were incubated with the sample solutions for 10 hours and washed 3 times with sterile 1X PBS. The mean fluorescence intensity per well was then

19

measured using a microplate reader and the cells were imaged using a fluorescent microscope. All fluorescence microscopy images were collected at the same exposure time.

Mean fluorescence intensity readings indicate significant differences in HEX+2 anti-HER2+2 IgGRb-TAMRA uptake between SK-BR-3 and MCF-7 cells. This result is expected, since SK-BR-3 cells overexpress the HER2 receptor, while MCF-7 cells do not. Additionally, there is a significant difference in uptake of nanocarriers with and without anti-HER2 antibodies for SK-BR-3 cells, as expected. Conversely, there is no significant difference in uptake of HEX-IgGRb between these two cell types. This result indicates that the nanocarrier may be effectively targeted to specific cell types through binding of targeting antibodies. Fluorescence intensity data is shown in Figure 7. Additional microscopy images are presented in Figures 8 and 9.
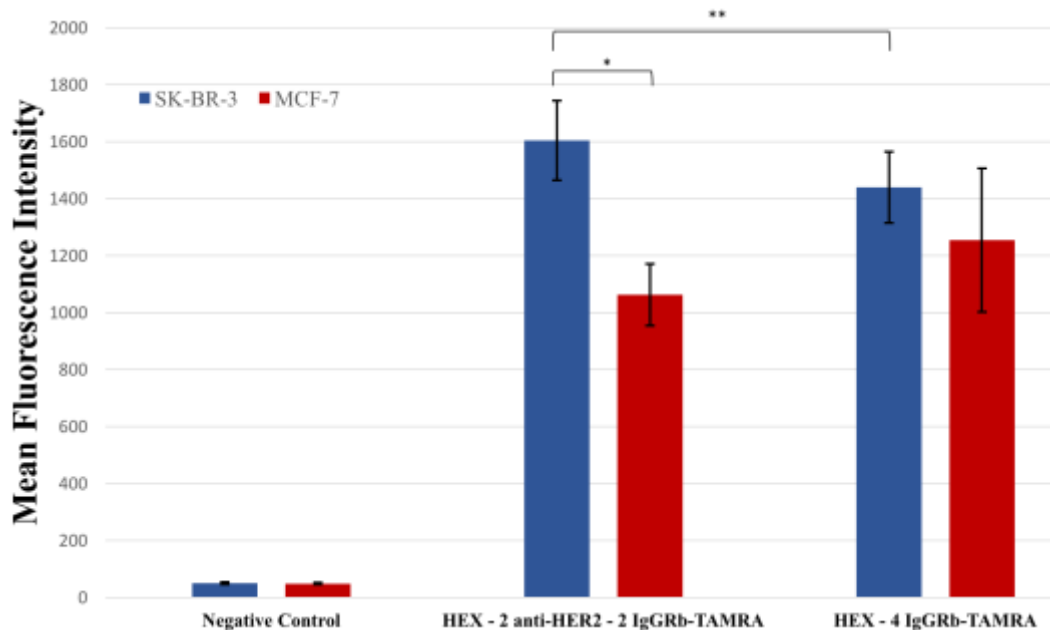

Figure 7. Mean fluorescence intensity data collected by microplate reader for SK-BR-3 and MCF-7 cells incubated with HEX nanocarriers bound to IgGRb-TAMRA or anti-HER2 + IgGRb-TAMRA. (* indicates p = 0.0004; ** indicates p < 0.0001; Significance threshold was set at p < 0.05).
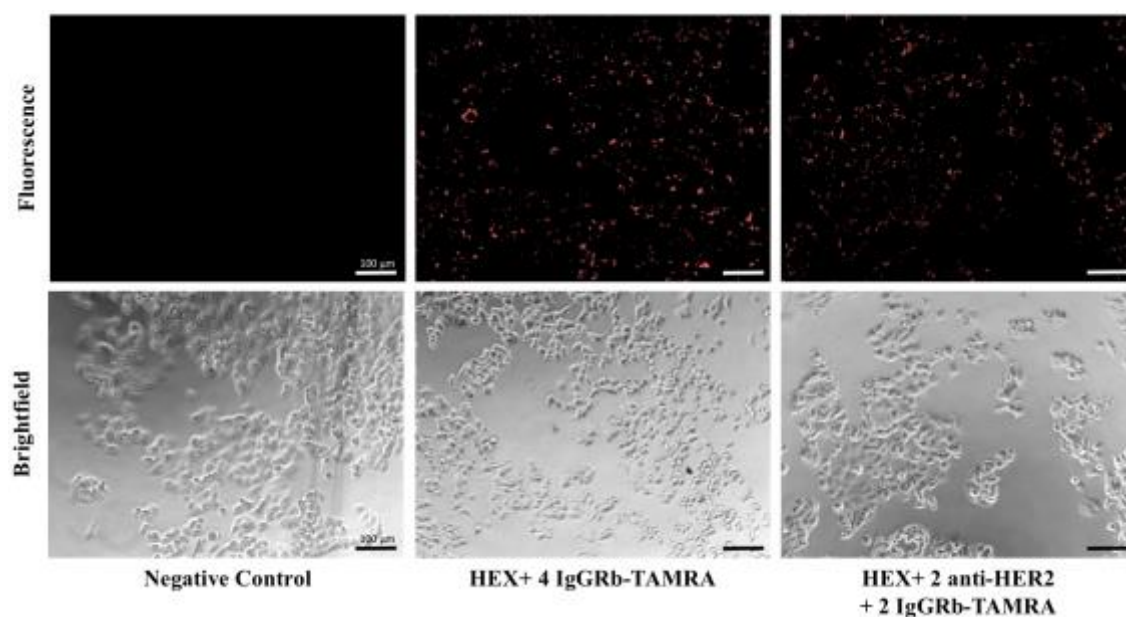
Figure 8. Microscopy images of MCF-7 cells following a 10-hour incubation with HEX nanocarriers bound to IgGRb-TAMRA or anti-HER2+IgGRb-TAMRA. The scale bar represents 100 μm.
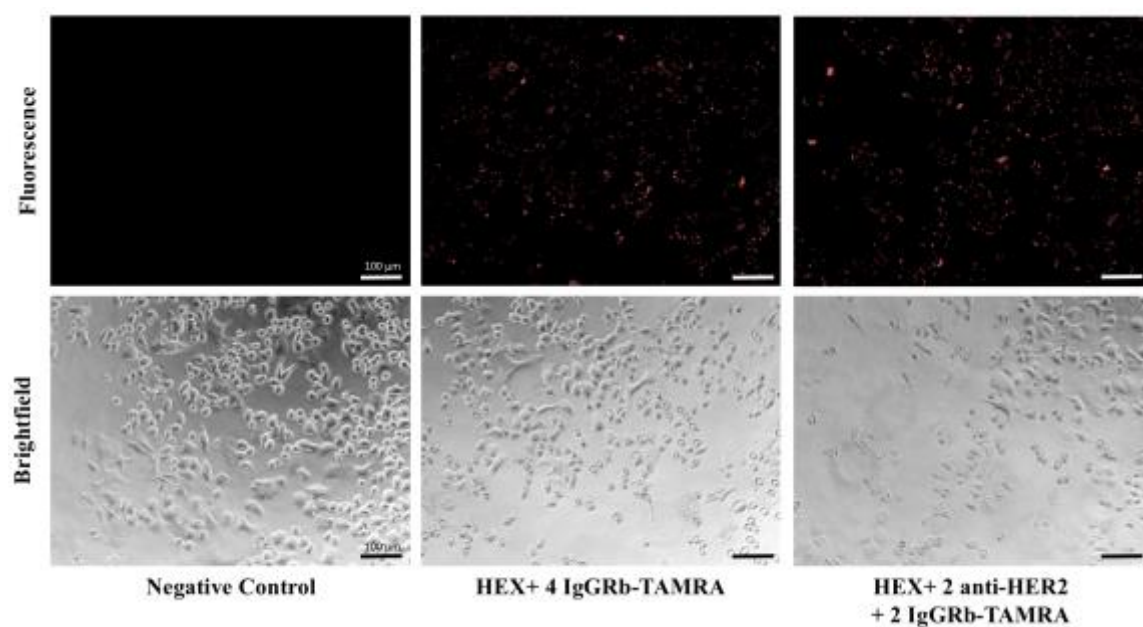

Figure 9. Microscopy images of SK-BR-3 cells following a 10-hour incubation with HEX nanocarriers bound to IgGRb-TAMRA or anti-HER2+IgGRb-TAMRA. The scale bar represents 100 μm.

CHAPTER 5

DISCUSSION AND CONCLUSIONS

We have successfully shown that both HEX and HEX-iRGD nanocarriers are capable of delivering functional antibodies to the intracellular environment of live cells. These nanocarriers are highly biocompatible and modular, easy to produce and maintain, and do not have a negative effect on cell viability or morphology. In the current study, we investigated two possible modifications to the original HEX nanocarrier with the goal of increasing targeting specificity. The functional nanocarriers HEX and HEX-iRGD were constructed from the recombinant proteins HEX-SPAB, SPAB-HEX, and SPAB-HEX-iRGD. High overall yield and purity of the recombinant proteins and assembled nanocarriers were confirmed through SDS-PAGE analysis.

The results of the IgGRb binding study confirmed the initial hypothesis that increasing the HEX:IgGRb ratio increases the size of the nanocarrier. However, the increase in size was not linear and coincided with broadening of the peaks, possibly indicating a diverse population of molecular species within a similar size range. The broad nature of the peaks at higher mixing ratios makes the average measured value harder to interpret, and it is yet unclear if there is any particular mixing ratio at which optimal saturation of HEX with IgGRb would be achieved. Future studies may include higher mixing ratios and different starting concentrations of HEX and IgGRb.

Cellular uptake studies indicate a significant level of uptake of both IgGRb-bound nanocarrier as well as unbound HEX by HeLa cells after a 24-hour incubation period. The results of the HEX + IgGRb cellular uptake study indicate a rather strong

concentration dependence of uptake, as evidenced by much higher intracellular fluorescent signals from cells incubated with higher concentrations of HEX + IgGRb. Further studies are necessary to determine an optimal concentration, which would allow for better uptake in a reduced incubation time.

Although HEX and IgGRb are very similar in size, HEX is readily internalized by HeLa cells, while IgGRb is not, as evidenced by the diffuse fluorescent signal of the IgGRb control. A possible explanation for this result is the relative shape of the hexameric self-assembling scaffold, which resembles a pore-forming complex. However, further investigation is needed to determine the molecular mechanisms of HEX uptake.

HEX-iRGD uptake by HeLa, MCF-7, and SK-BR-3 cells differed from HEX uptake in terms of both the intensity of signal from internalized nanocarriers as well as the pattern of the signal. Overall, all three cell lines internalized HEX-iRGD more readily, although images MCF-7 and SK-BR-3 cells do show an intense signal around the outside of some cells. Results of the integrin specific targeting study indicate no difference in membrane interaction patterns of HEX and HEX-iRGD when in the presence of anti-integrin $\alpha v \beta 3$ antibodies, suggesting that integrin targeting is not effective. These results may be a consequence of the iRGD domains affecting the interactions between HEX and the cell membrane.

The failure of HEX-iRGD to achieve targeting specificity may be due to several factors, with the most probable being steric hindrance of the iRGD peptide by linkers, SPAB domains, as well as bound antibodies in the assembled functional nanocarrier. To investigate this hypothesis, it may be worthwhile modifying the original HEX nanocarrier with iRGD domains that are connected via flexible linkers, similar to those connecting

HEX to the SPAB domains. A representative diagram of the HEX nanocarrier is shown in Figure A7.

Another possible explanation for the apparent lack of iRGD function may be the relatively large size of antibody-bound HEX-iRGD, as large particles may have difficulty interacting with NRP-1 following integrin binding. However, this hypothesis is not supported by literature results, since a recent study has shown significant increase in tumor-selective accumulation and penetration of iRGD-functionalized polymersomes, indicating that iRGD effects on targeting and internalization are applicable to larger nanoparticles [23].

HER2 receptor targeting, however, does show promise and should be investigated further. This approach to targeting does not require any modifications of the original HEX nanocarrier, and is therefore simpler than the introduction of additional targeting domains. However, given the covalent nature of the binding between the SPAB domain of the nanocarrier and antibodies, it may prove difficult to achieve a truly homogeneous population of particles. Although the HEX nanocarrier is introduced into a solution that has the desired concentration ratio of targeting antibodies to intracellular antibodies, it is essentially impossible to guarantee that each HEX nanocarrier contains the desired amount of targeting and intracellular antibodies. This notion, although an advantage in terms of carrier fabrication and preparation, may prove a disadvantage for future *in vivo* investigations.

CHAPTER 6

FUTURE WORK

Additional studies are necessary to evaluate the stability of HEX + Antibody at higher loading ratios and working concentrations. Our preliminary data indicate that at certain higher ratios and concentrations, the antibody-bound nanocarriers may form aggregates, which potentially hinders uptake and targeting, and may present a significant limitation for future *in vivo* studies. Studies in the near future should investigate the stability of antibody-bound HEX at higher concentrations and ratios that were previously shown to be therapeutically relevant. DLS may be used as an initial "quality check" method to evaluate stability and aggregation over time, but additional methods, such as size-exclusion chromatography and analytical ultracentrifugation should also be considered for evaluation of stability and particle size distribution over time.

To further investigate the reasons for the failure of the iRGD targeting approach, it may be worthwhile engineering a HEX nanocarrier with iRGD-domains connected via flexible linkers to reduce steric effects and promote iRGD-integrin interactions. If iRGD targeting still does not show significant differences, the original HEX nanocarrier may be bound to anti-integrin $\alpha v \beta 3$ antibodies to test whether integrin targeting is an effective strategy for our nanocarrier design.

The next tasks involve delivery of an intracellular therapeutic antibody to cells representing a certain disease model. Future studies should utilize HEX nanocarriers bound to a combination of targeting antibodies as well as antibodies that will have the desired therapeutic effect once delivered to the cytosol. Effect of these antibodies may be

evaluated by measuring cell viability via MTT assay or live-dead staining, or as an alternative, a western blot may be used to show successful binding of the delivered antibody to its cytosolic target protein.

In the long term, it may be worth investigating the use of a combination of targeting antibodies to increase delivery specificity. Many disease models, such as cancer cells, are known to overexpress numerous key receptors that may present excellent extracellular protein targets. Theoretically, using a combination of targeting antibodies should increase the likelihood of successful targeting, but in certain cases, it may also lead to increased off-site effects. The effectiveness of this approach should first be evaluated *in vitro* to determine whether it holds promise for potential *in vivo* trials.
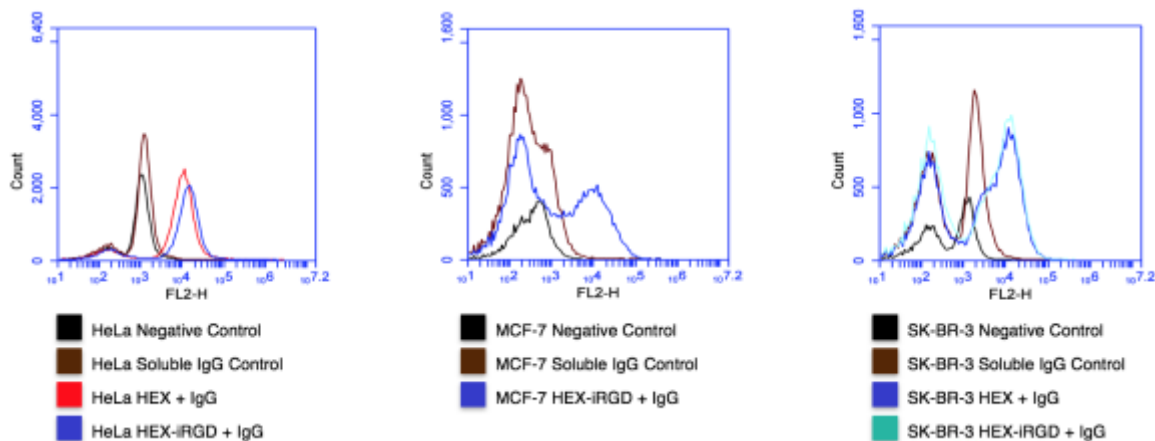
APPENDIX A

ADDITIONAL FIGURES

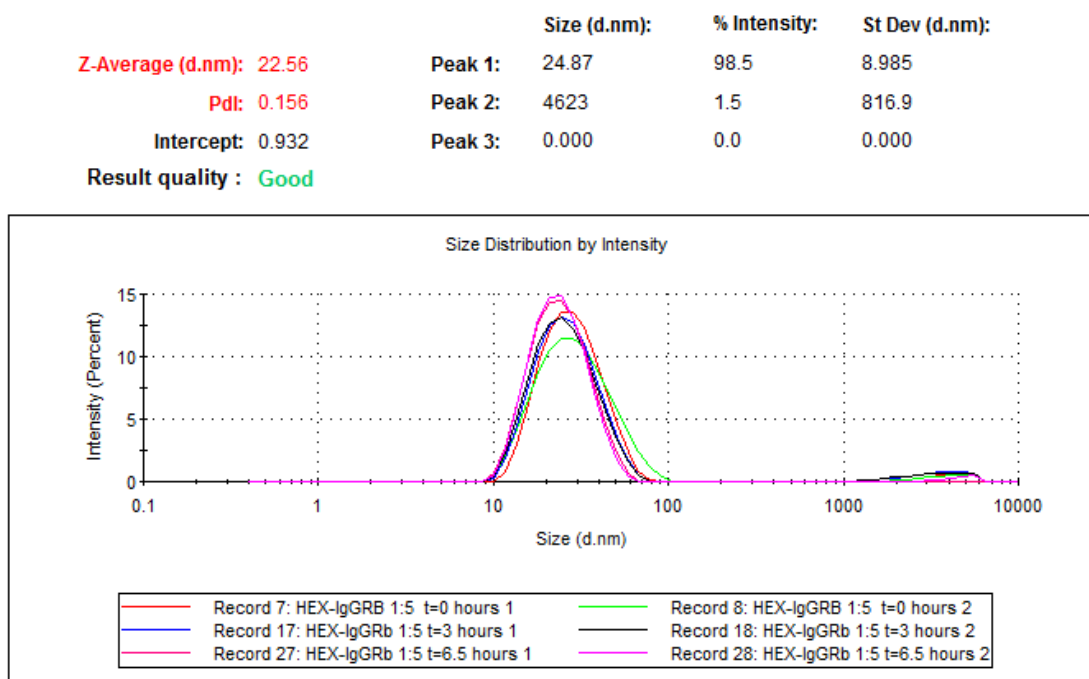**Figure A1**. Flow cytometry analysis of HEX + IgGRb and HEX-iRGD + IgGRb uptake by HeLa, MCF-7, and SK-BR-3 cells.

Figure A2. DLS time course data for stability of HEX + IgGRb when mixed at a 1:5 ratio of HEX to IgGRb.

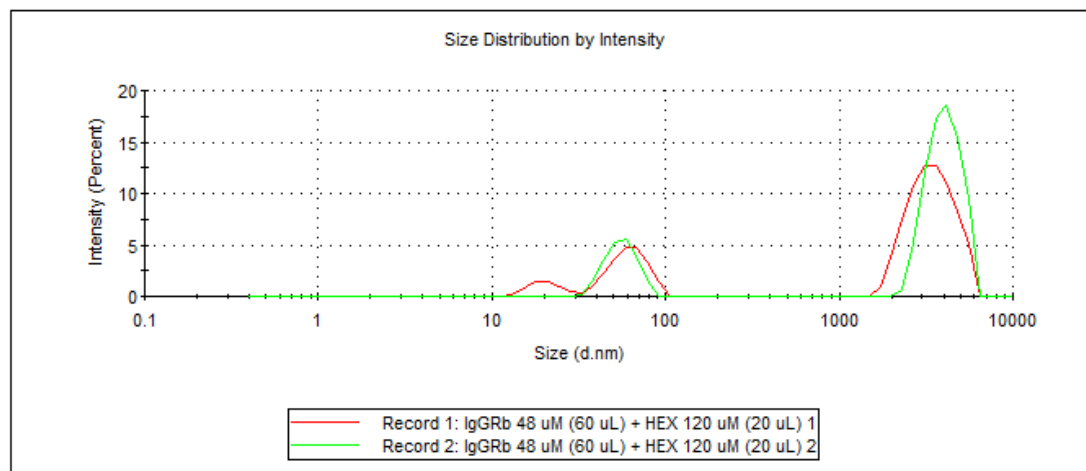|	Size (d.nm):	% Intensity:	St Dev (d.nm):
Z-Average (d.nm): 316.8	Peak 1: 3484	72.6	994.1
Pdl: 1.000	Peak 2: 61.76	21.4	14.40
Intercept: 0.832	Peak 3: 20.89	6.0	4.994
Result quality : Refer to quality report			

Figure A3. Size distribution by intensity of concentrated HEX (30 µM) + IgGRb (36 µM) at t = 0 hours.

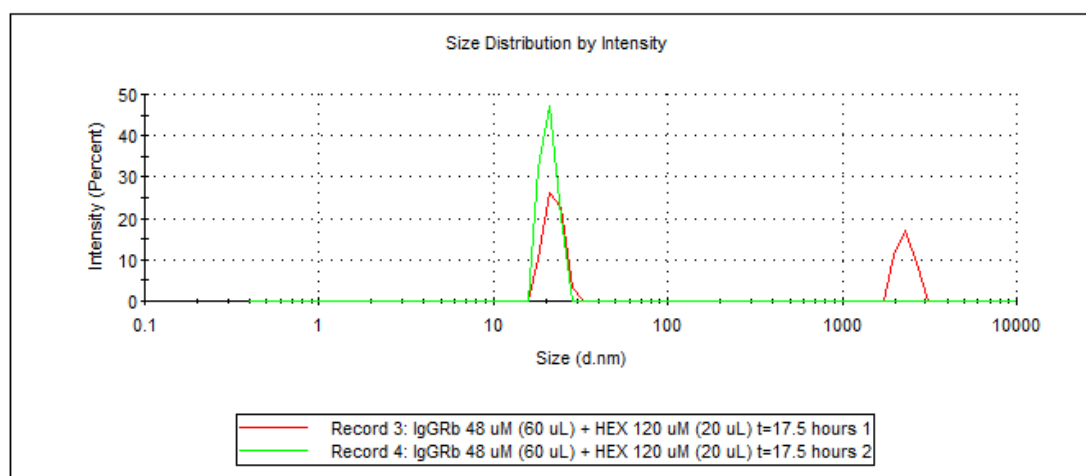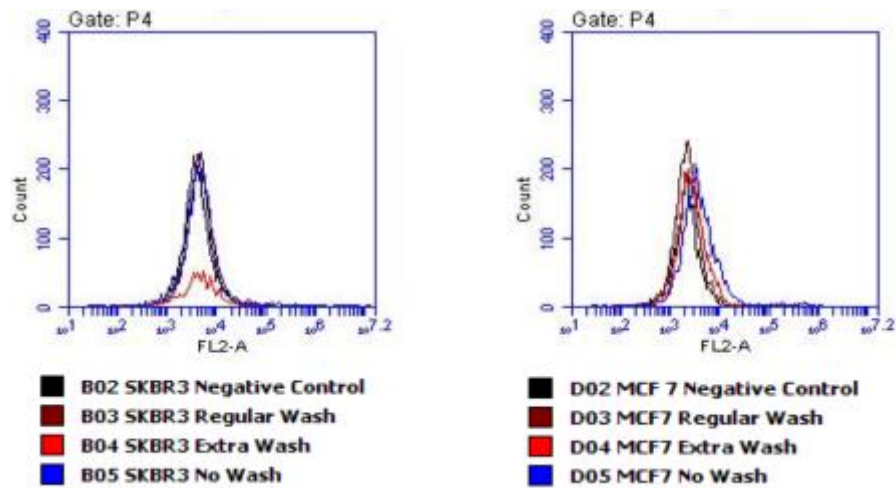|	Size (d.nm):	% Intensity:	St Dev (d.nm):
Z-Average (d.nm): 3204	Peak 1: 20.79	100.0	2.203
Pdl: 1.000	Peak 2: 0.000	0.0	0.000
Intercept: 0.767	Peak 3: 0.000	0.0	0.000
Result quality : Refer to quality report			

Figure A4. Size distribution by intensity of concentrated HEX (30 µM) + IgGRb (36 µM) at t = 17.5 hours.

Sample	SK-BR-3 Mean FL2-A	MCF-7 Mean FL2-A
Negative Control	5,223.16	2,524.83
Regular Wash	6,792.81	3,126.87
Extra Wash	5,973.01	3,376.03
No Wash	32,341.23	11,032.01

Figure A5. Flow cytometry data for the washing protocol efficiency study. Regular wash refers to 3X wash with 1X PBS, while Extra Wash refers to 7X wash with 1X PBS.
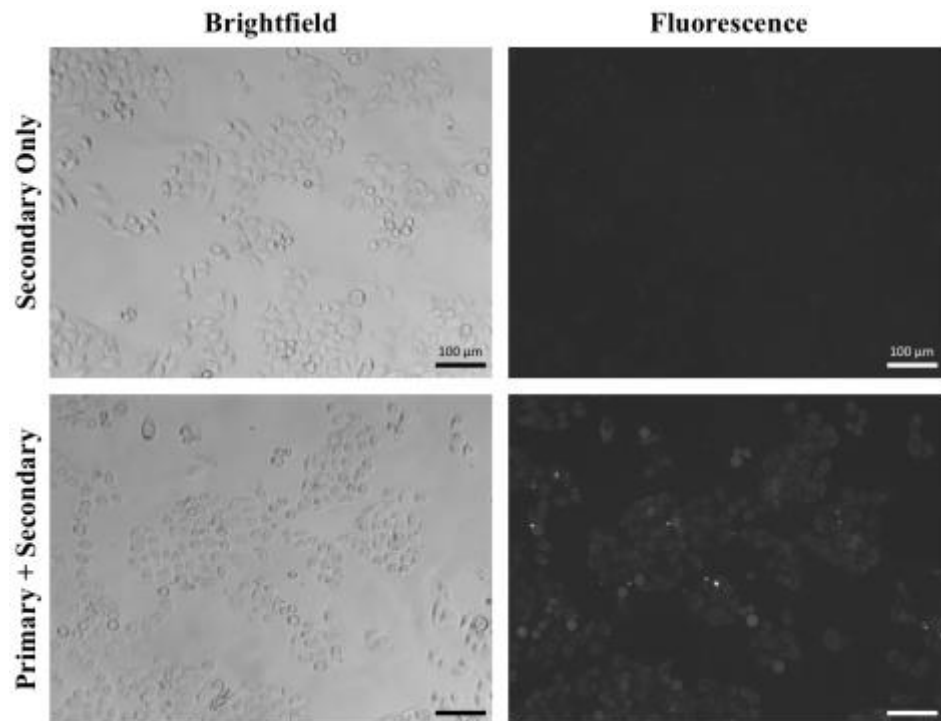

Figure A6. Fluorescence microscopy images showing successful integrin blocking by the primary anti-integrin αvβ3 antibodies that were subsequently labeled with a secondary anti-rabbit-FITC antibody. The scale bar represents 100 μm.
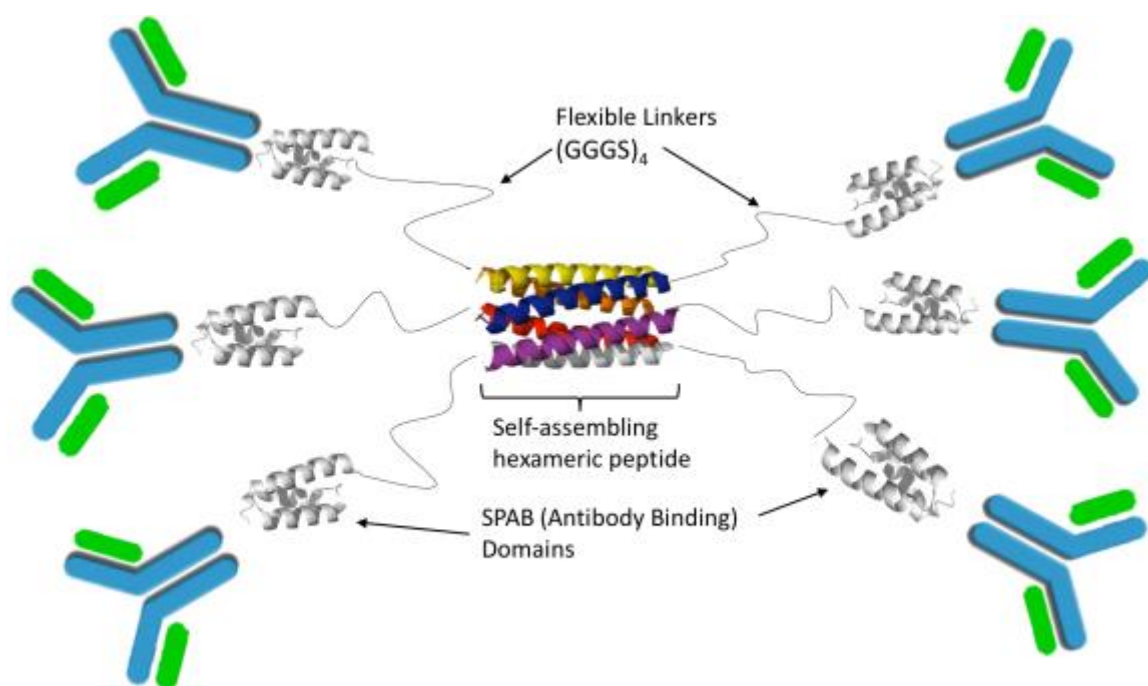
Figure A7. Representative diagram of antibody-bound HEX nanocarrier structure. *** Note: not drawn to scale (molecular weight of HEX nanocarrier: ~ 76 kDa, molecular weight of 1 IgG: ~ 150 kDa)

REFERENCES

1. National Cancer Institute (2016). [Statistical Information on cancer mortality rates and prevalence]. Retrieved from: http://www.cancer.gov/about-cancer/what-is-cancer/statistics

2. Jerjian, T. V., Glode, A. E., Thompson, L. A., & O'Bryant, C. L. (2016). Antibody-Drug Conjugates: A Clinical Pharmacy Perspective on an Emerging Cancer Therapy. *Pharmacotherapy, 36*(1), 99-116. doi:10.1002/phar.1687

3. Palanca-Wessels, M. C., Booth, G. C., Convertine, A. J., Lundy, B. B., Berguig, G. Y., Press, M. F., . . . Press, O. W. (2016). Antibody targeting facilitates effective intratumoral siRNA nanoparticle delivery to HER2-overexpressing cancer cells. *Oncotarget*. doi:10.18632/oncotarget.7076

4. Lehar, S. M., Pillow, T., Xu, M., Staben, L., Kajihara, K. K., Vandlen, R., . . . Mariathasan, S. (2015). Novel antibody-antibiotic conjugate eliminates intracellular S. aureus. *Nature, 527*(7578), 323-328. doi:10.1038/nature16057

5. Li, J. Y., Perry, S. R., Muniz-Medina, V., Wang, X., Wetzel, L. K., Rebelatto, M. C., . . . Coats, S. R. (2016). A Biparatopic HER2-Targeting Antibody-Drug Conjugate Induces Tumor Regression in Primary Models Refractory to or Ineligible for HER2-Targeted Therapy. *Cancer Cell, 29*(1), 117-129. doi:10.1016/j.ccell.2015.12.008

6. Niikura, K., Horisawa, K., & Doi, N. (2016). Endosomal escape efficiency of fusogenic B18 and B55 peptides fused with anti-EGFR single chain Fv as estimated by nuclear translocation. *J Biochem, 159*(1), 123-132. doi:10.1093/jb/mvv083

7. Guo, K., Li, J., Tang, J. P., Tan, C. P., Hong, C. W., Al-Aidaroos, A. Q., . . . Zeng, Q. (2011). Targeting intracellular oncoproteins with antibody therapy or vaccination. *Sci Transl Med, 3*(99), 99ra85. doi:10.1126/scitranslmed.3002296

8. Weiner, G. J. (2015). Building better monoclonal antibody-based therapeutics. *Nat Rev Cancer, 15*(6), 361-370. doi:10.1038/nrc3930

9. Lim, S. I., Lukianov, C. I., & Champion, J. A. (2017). Self-assembled protein nanocarrier for intracellular delivery of antibody. *Journal of Controlled Release*.

10. Zhao, Y., Ji, T., Wang, H., Li, S., Zhao, Y., & Nie, G. (2014). Self-assembled peptide nanoparticles as tumor microenvironment activatable probes for tumor targeting and imaging. *J Control Release, 177*, 11-19. doi:10.1016/j.jconrel.2013.12.037

11. Itakura, S., Hama, S., Ikeda, H., Mitsuhashi, N., Majima, E. and Kogure, K. (2015), Effective capture of proteins inside living cells by antibodies indirectly linked to a novel cell-penetrating polymer-modified protein A derivative. FEBS Journal, 282: 142–152. doi: 10.1111/febs.13111

12. Bale, S. S., Kwon, S. J., Shah, D. A., Banerjee, A., Dordick, J. S., & Kane, R. S. (2010). Nanoparticle-mediated cytoplasmic delivery of proteins to target cellular machinery. *Acs Nano*, *4*(3), 1493-1500.

13. Abraham, A., Natraj, U., Karande, A. A., Gulati, A., Murthy, M. R., Murugesan, S., ... & Savithri, H. S. (2016). Intracellular delivery of antibodies by chimeric Sesbania mosaic virus (SeMV) virus like particles. *Scientific reports*, *6*, 21803.

14. Sha, H., Zou, Z., Xin, K., Bian, X., Cai, X., Lu, W., . . . Liu, B. (2015). Tumor-penetrating peptide fused EGFR single-domain antibody enhances cancer drug penetration into 3D multicellular spheroids and facilitates effective gastric cancer therapy. *J Control Release, 200*, 188-200. doi:10.1016/j.jconrel.2014.12.039

15. Teesalu, T., Sugahara, K. N., & Ruoslahti, E. (2013). Tumor-penetrating peptides. *Front Oncol, 3*, 216. doi:10.3389/fonc.2013.00216

16. Zaccai, N. R., Chi, B., Thomson, A. R., Boyle, A. L., Bartlett, G. J., Bruning, M., . . . Woolfson, D. N. (2011). A de novo peptide hexamer with a mutable channel. *Nat Chem Biol, 7*(12), 935-941. doi:10.1038/nchembio.692

17. Unverdorben, F., A. Farber-Schwarz, F. Richter, M. Hutt and R. E. Kontermann (2012). Half-life extension of a single-chain diabody by fusion to domain B of staphylococcal protein A. *Protein Eng Des Sel 25*(2): 81-88.

18. Thermo Scientific (2015). [Description of NanoDrop 2000 instrument]. Retrieved from: http://www.nanodrop.com/Productnd2000overview.aspx

19. GE Healthcare Life Sciences (2015). [Description of PD-10 Desalting Column] Retrieved from: https://www.gelifesciences.com/gehcls_images/GELS/Related%20Content/Files/1314723116657/litdoc52130800BB_20110830191706.pdf

20. Malvern Instruments (2015). [Description of Zetasizer Nano instrument]. Retrieved from: http://www.malvern.com/en/products/product-range/zetasizer-range/zetasizer-nano-range/defaultb.aspx

21. GE Healthcare Life Sciences (2015). [Description of ÄKTA fast protein liquid chromatography system] Retrieved from: http://www.gelifesciences.com/webapp/wcs/stores/servlet/catalog/en/GELifeSciences-us/products/AlternativeProductStructure_17162/18664501

22. National Cancer Institute (2017). [A Story of Discovery: HER2's Genetic Link to Breast Cancer Spurs Development of New Treatments] Retrieved from: https://www.cancer.gov/research/progress/discovery/HER2

23. Simón-Gracia, L., Hunt, H., Scodeller, P., Gaitzsch, J., Kotamraju, V. R., Sugahara, K. N., Teesalu, T. (2016). iRGD peptide conjugation potentiates intraperitoneal tumor delivery of paclitaxel with polymersomes. *Biomaterials*, *104*, 247-257.

VITA

Cyril I. Lukianov

Cyril Lukianov was born in Mogilev, Belarus, where he grew up and lived until age 11. In 2005, his family immigrated to the United States, where he currently resides. He lived in Brooklyn, New York, and Atlanta, Georgia, a charming southern city he calls home. He attended the University of Vermont and the University of Georgia as a biochemistry major, before deciding to pursue biomolecular engineering and transferring to Georgia Tech. When he is not studying, or working in the lab, Cyril enjoys reading, music, and road biking.